

Inclusive pion double charge exchange in light p -shell nuclei

W. Fong,^{*} J. L. Matthews, M. L. Dowell,[†] E. R. Kinney,[‡]

T. Soos,[§] M. Y. Wang,[¶] and S. A. Wood^{**}

*Department of Physics and Laboratory for Nuclear Science
Massachusetts Institute of Technology, Cambridge MA 02139*

P. A. M. Gram^{††}

Los Alamos National Laboratory, Los Alamos NM 87545

G. A. Rebka, Jr. and D. A. Roberts^{‡‡}

Department of Physics, University of Wyoming, Laramie, Wyoming 82071

(Dated: July 16, 2021)

Abstract

We report the results of a series of measurements of the differential cross sections for inclusive pion double charge exchange in ${}^6,7\text{Li}$, ${}^9\text{Be}$, and ${}^{12}\text{C}$ for positive and negative incident pions of energies 120, 180, and 240 MeV. The data are compared with the predictions of an intranuclear cascade model and a model based on two sequential single charge exchange processes.

^{*}Present Address: Varian Medical Systems, Palo Alto, CA 94304

[†]Present Address: Optoelectronics Division, National Institute of Standards and Technology, Boulder, CO 80305

[‡]Present Address: Department of Physics, University of Colorado, Boulder, CO 80309

[§]Present Address: 1255 Marina Point, Casselberry, FL 32707

[¶]Present Address: The RAND Corporation, Santa Monica, CA 90406

^{**}Present Address: Thomas Jefferson National Accelerator Facility, Newport News, VA 23606

^{††}Present Address: 82-1021 Kaimalu Place, Captain Cook, HI 96704

^{‡‡}Present Address: Department of Radiation Oncology, University of Michigan Medical School, Ann Arbor, MI 48109

I. INTRODUCTION

The study of pion double charge exchange (DCX) has been pursued with the aim of elucidating the mechanisms of multiple pion interactions in nuclei. Whatever the details of the mechanism, this reaction must at least result in the charges of two nucleons being changed. Indeed, it has been found that the simplest picture of the reaction, in which it proceeds by successive single charge exchanges (see Fig. 1), provides a qualitative explanation of the systematics that are observed [1].

Serious investigation of the inclusive DCX reaction began in 1980, with the first measurement using modern equipment of the doubly differential cross section for $^{16}\text{O}(\pi^+, \pi^-)X$ at three angles with 240 MeV pions performed at SIN (now PSI) [2]. Subsequently, an extensive series of measurements of inclusive double charge exchange cross sections was carried out at the Los Alamos Meson Physics Facility [3, 4, 5, 6, 7, 8, 9]. The (π^-, π^+) reaction was studied in ^3He , and the (π^\pm, π^\mp) reactions in nine nuclei: ^4He , $^{6,7}\text{Li}$, ^9Be , ^{12}C , ^{16}O , ^{40}Ca , ^{103}Rh , and ^{208}Pb . Doubly differential cross sections were measured for each target over the outgoing pion energy range from 10 MeV up to the kinematic limit, at three to five angles for incident pion energies in the range from 120 to 270 MeV. Some 300 pion energy spectra have been obtained with good statistics and absolute accuracies of 10-15%.

The systematics of the reaction in ^{16}O , ^{40}Ca , ^{103}Rh , and ^{208}Pb revealed by these experiments has been previously discussed [3]. Briefly, it is found that only in ^{16}O do the doubly differential cross sections much resemble the most likely phase space distribution (that containing a pion, two nucleons and a residual nucleus) or, in fact, any other reasonable distribution generated by assuming that the mechanism is governed by a constant matrix element. In the heavier nuclei the distribution of outgoing pions is strongly peaked toward lower energies and depleted at higher energies when compared to the phase space distribution.

The doubly differential cross sections for DCX in ^3He and ^4He exhibited striking double peaked outgoing pion energy spectra at forward angles (25° , 50°) that evolved into a single peak distribution as the angle of observation reached 130° . This feature was most pronounced at an incident energy of 240 MeV, but persisted at incident energies down to 150 MeV in ^4He [7] and 120 MeV in ^3He [4].

In this paper we report measurements of the doubly differential cross section for inclusive

DCX in the light p -shell nuclei ${}^6,{}^7\text{Li}$, ${}^9\text{Be}$, and ${}^{12}\text{C}$. These observations will serve to trace the evolution of the double peaked structure into a nearly featureless spectrum as the complexity of the target nucleus is increased. A second objective of the present work was to investigate, by comparing the (π^+, π^-) reactions in ${}^6\text{Li}$ and ${}^7\text{Li}$, the effect on the DCX cross section of a single extra neutron in the target nucleus.

Only fragmentary data for DCX in these nuclei existed prior to the present measurement. Gilly *et al.* have reported a few measurements at 0° for (π^+, π^-) in Li and Be [10] and (π^-, π^+) in ${}^7\text{Li}$, ${}^9\text{Be}$, and ${}^{12}\text{C}$ [11], at incident energies in the 200 MeV region. Batusov *et al.* measured total DCX cross sections for 80 MeV π^+ on Be and Al and 140 MeV π^- on Be and C [12]. Using a propane bubble chamber, Massue *et al.* measured total cross sections for (π^+, π^-) in ${}^{12}\text{C}$ at 138, 204, and 228 MeV [13]. Evseev *et al.* measured a π^+ spectrum at 30° for 107 MeV π^- on ${}^7\text{Li}$, but with poor statistical accuracy [14].

Subsequent to the measurements discussed in the present paper, forward-angle cross sections for the (π^-, π^+) reaction on ${}^6,{}^7\text{Li}$ and ${}^{12}\text{C}$ at incident energies 0.59, 0.75, and 1.1 GeV have been reported [15].

II. EXPERIMENTAL APPARATUS AND PROCEDURE

In the present experiment, the inclusive DCX processes (π^\pm, π^\mp) have been investigated by measuring the doubly differential cross sections, $d^2\sigma/d\Omega dE_\pi$, at three to five angles in the range 25° – 130° , for incident pion energies between 120 and 240 MeV. At each angle, the range of outgoing pion energies from 10 MeV up to the kinematic limit for each reaction was covered. Preliminary results of this experiment were reported in Ref. [9].

The experiment was performed with incident π^\pm beams from the high-energy pion channel (“P3”) at the Los Alamos Meson Physics Facility. The outgoing pions were detected using a 180° vertical bend, double focusing magnetic spectrometer, with an effective solid angle of about 16 msr and a momentum bite of about 8%, as shown in Fig. 2. The experimental apparatus and procedure have been discussed in detail by Wood *et al.* [3], Yuly *et al.* [4], and Kinney *et al.* [7] and will be treated only briefly here.

The detector system had five components: a wire chamber (WC0) placed in the mid-plane of the spectrometer, two wire chambers (WC1 and WC2) near the focal plane that were used to reconstruct trajectories, a 1.6 mm scintillator (S1) behind WC1 and WC2 that

provided an accurate time reference for the trigger as well as pulse height information, and a fluorocarbon (FC-88) Čerenkov detector that distinguished electrons from pions.

The trigger was a fourfold coincidence among the three wire chambers and the scintillator. Inclusion of WC0 guaranteed that a particle had passed through the spectrometer. The timing information available from this chamber was also used to distinguish pions from very slow protons.

All of the targets (${}^6\text{Li}$, ${}^7\text{Li}$, ${}^9\text{Be}$, ${}^{12}\text{C}$) in this experiment were solid rectangular slabs. In addition, a polyethylene (CH_2) target was employed to simultaneously normalize both the beam flux and spectrometer acceptance by observing elastic πp scattering. The targets were mounted in aluminum frames on a ladder that could be raised or lowered (to place the target of interest in the incident beam) and rotated about the vertical axis (to orient the plane of the target at an appropriate angle with respect to the beam).

Before reaching the target, the pion beam passed through an ionization chamber that was used to determine the relative flux. Since this device was sensitive to all charged particles in the beam, it was necessary to normalize the flux measurement each time the beam transport elements were adjusted. Downstream of the target the pion beam impinged on a CH_2 slab from which pions scattered at 90° on each side of the beam were detected by scintillator telescopes, in order to monitor the position of the incident beam and to provide a cross-check of the ionization chamber.

To measure the doubly differential DCX cross sections each target was exposed to an incident pion beam and events were recorded at a series of spectrometer momentum settings until the measured statistical uncertainties in the number of detected pions were approximately 5%. Data were collected at 10 MeV intervals in outgoing pion energy. In addition, background observations were made at a selected set of spectrometer settings using an empty target frame. Each time the incident pion charge or energy was changed, a series of CH_2 normalizations was performed.

III. DATA ANALYSIS

The goal of this experiment was to measure a doubly differential cross section for each reaction, incident pion energy, scattering angle, and outgoing pion energy. The doubly

differential cross section is related to observable quantities as follows:

$$\frac{d^2\sigma}{d\Omega dE_\pi} = \frac{N_{\text{det}} \epsilon_c}{N_{\text{inc}} x \rho f_d f_l \Delta\Omega \Delta E_\pi} \quad (1)$$

where N_{det} is the number of pions detected, N_{inc} is the number of incident pions, x is the effective thickness of the target, ρ is the target density, $\Delta\Omega$ is the effective solid angular acceptance, ΔE_π is the range of outgoing pion energy, ϵ_c is the correction of the spectrometer acceptance due to multiple scattering and energy loss, f_d is the correction due to pion decay, and f_l is the dead-time correction.

The analysis procedure is described in detail in Ref. [8] and will only be summarized here. (See also Refs. [4, 7].)

A. Wire chamber calibration and phase space definition

Calibration constants relating time differences of the signals from the wire chambers to positions on the focal plane were established by placing a collimated ^{55}Fe source at precisely measured positions in front of the chambers. In the data analysis, the position information from WC1 and WC2 for each event was used to reconstruct the particle trajectory back to the focal plane of the spectrometer. Reconstructed trajectories were tested for conformity with the distribution in phase space of particles that could have been transmitted by the spectrometer from the target to the focal plane.

B. Particle Identification

Positive pions and protons were generally distinguished on an event-by-event basis by means of their different pulse heights in the scintillator, or, in some cases, by their time-of-flight between WC0 and S1.

Since pions and electrons¹ both emit Čerenkov radiation in FC-88 at spectrometer settings greater than 180 MeV/c ($T_\pi = 88$ MeV), it was not possible to use the Čerenkov detector to distinguish electrons from pions on an event-by-event basis. Instead, a statistical method

¹ Electrons or positrons, depending on the charge setting of the spectrometer. The word “electron” will be used generically throughout this discussion.

was used, which is described in detail in Ref. [8] and is very similar to that described in Ref. [4].

C. Acceptance and Dispersion

The momentum acceptance, $\Delta p/p$, and dispersion were determined by changing the spectrometer magnetic field to move a πp elastic scattering peak across the spectrometer focal plane. The relative acceptance as a function of focal plane position obtained by this method was used to correct N_{det} . The effective total momentum acceptance was determined to be about 8% by integration across the entire focal plane.

D. Normalization

The absolute number of incident pions, N_{inc} in Eq. (1), was obtained by comparison of πp elastic scattering measurements with known cross sections determined from the energy-dependent phase shift program SCATPI [16]. The effective total solid angle, $\Delta\Omega$, was included in this calibration. This procedure was repeated at several scattering angles for each setting of the beam transport system in order to improve the accuracy of the normalization, as well as to check for the presence of angle-dependent systematic errors.

E. Background Subtraction

A linear interpolation between the spectrometer momentum settings at which empty-frame (background) measurements were made was used to obtain the background contribution which was then subtracted from the raw DCX spectra. The largest backgrounds occurred at the lowest measured outgoing pion energy of 10 MeV and were about 25% of the foreground.

F. Corrections

Corrections were made to account for other effects that would change the shape and magnitude of the measured cross sections. The number of pions detected was reduced by decay as they traveled from the target to the detectors. Approximately 80% of the pions

survived at 200 MeV, while at 10 MeV only 30% survived. Some of the decay muons traversed the spectrometer, while others did not. Moreover, it was possible for pions emerging from the target that would not have traversed the spectrometer to decay into muons that could do so. Since the detector system could not separate the muons from pions, these effects were accounted for by Monte Carlo methods which produced the factor f_d in Eq. (1). This procedure is described in detail in Refs. [3, 17]. The fraction of muon contamination ranges from 1% at 10 MeV to 20% at 200 MeV outgoing pion kinetic energy.

Energy loss and multiple scattering in the target and in WC0 changed the effective acceptance of the spectrometer; these were corrected for by the factor ϵ_c , which was determined by simulation to be different from unity only for outgoing pion energies less than 30 MeV. The maximum value of ϵ_c was about 1.3.

G. Integrated cross sections

Integration of the doubly differential cross sections over outgoing pion energy, using the trapezoid rule, yielded an angular distribution. The angular distributions were fitted with sums of Legendre polynomials, which were integrated to determine a quantity which we term the “total reaction cross section.” The uncertainties in these procedures are discussed in Ref. [8] and were less than, or comparable to, the systematic uncertainties discussed in the next section.

H. Systematic uncertainties

The uncertainty in the normalization of the cross section contains contributions from uncertainties in the thicknesses of the targets (2–3%) and in the phase shift prediction of the free πp cross section (2%) [16]. The uncertainty in the determination of a particle’s position in the spectrometer focal plane and of the spectrometer acceptance function are each estimated to be 1%. For the measurements at 180 MeV and 240 MeV there is an additional 4% uncertainty in a correction for trigger inefficiency. The uncertainties due to the determination of electronics deadtime, spectrometer dispersion, and wire chamber efficiency were insignificant compared to those listed above. In addition, there is an uncertainty due to slowly varying changes in the response of the ionization chamber used to monitor the incident

beam flux. These variations were monitored by comparison with the primary proton beam monitor and the downstream scattering monitor, and were observed to occur on roughly the same time scale as changes of spectrometer angle. The resulting uncertainty is thus treated as an angle-dependent uncertainty.

There are also uncertainties that depend on the outgoing pion energy. These include contributions from the electron-pion separation procedure, which were between 2% and 5%, from estimates of the corrections for energy loss and multiple scattering in the target and in the mid-spectrometer wire chamber, and from effects of pion decay and muon contamination, which contributed an additional 5%.

Table I lists the systematic uncertainties for each incident beam.

I. Pion-induced pion production

For incident pion energies above about 170 MeV, detection of an outgoing pion of charge opposite to that of the incident pion no longer provides a unique signature of DCX, as the processes $n(\pi^+, \pi^-)\pi^+p$ or $p(\pi^-, \pi^+)\pi^-n$ can occur on one of the target nucleons. Although the contribution of pion-induced pion production (PIPP) is negligible (see Ref. [17]) for incident energy 180 MeV, this effect must be taken into account at 240 MeV.

To estimate the contribution of PIPP, we follow the procedure used in Ref. [7]. Assuming that PIPP in a nucleus occurs as a quasi-free process on a single nucleon, the effects of absorption and other competing π -nucleus reactions and of the nuclear medium are taken into account by multiplying the free nucleon PIPP cross section by an “effective” number of nucleons, N_{eff} . An extensive study of π -nucleus reactions was reported by Ashery *et al.*[18], from which values of N_{eff} were extracted. These authors found that N_{eff} for positive (negative) incident pions exhibited a universal, energy-independent power-law dependence on Z (N). Moreover, the incident energy dependence of N_{eff} was found to be very similar for all target nuclei. These two results allow us to obtain, by interpolation, values of N_{eff} for ${}^6,7\text{Li}$, ${}^9\text{Be}$, ${}^{12}\text{C}$, and ${}^{16}\text{O}$ for incident π^\pm energy 240 MeV.

Precise measurements of the $\pi^-p \rightarrow \pi^-\pi^+n$ cross section have been reported by Bjork *et al.*[19]. The observed[20] equality of the $\pi^+d \rightarrow \pi^+\pi^-pp$ and $\pi^-d \rightarrow \pi^-\pi^+nn$ cross sections, and of the $\pi^-d \rightarrow \pi^-\pi^+nn$ and $\pi^-p \rightarrow \pi^-\pi^+n$ cross sections, justifies using the results of Bjork *et al.*[19] for both positive and negative incident pions. This procedure yields the

values of PIPP cross sections given in Table II.

Although extensive studies of the differential cross sections for PIPP in nuclei have been carried out, *e.g.*, most recently by the CHAOS collaboration [21], few total cross sections have been quoted. Rahav *et al.* [22] observed the $^{12}\text{C}(\pi^-, \pi^+\pi^-)$ reaction at 292 MeV, and Grion *et al.* [23] observed the $^{16}\text{O}(\pi^+, \pi^+\pi^-)$ reaction at 280 MeV. Unfortunately, these results are inconsistent when rescaled using a reasonable energy and A -dependence (see Ref. [3]). Rahav *et al.* speculate that the discrepancy may arise from the methods used to extrapolate the data to obtain a total reaction cross section. They point out that the fraction of phase space covered in their work is 43 times larger than that covered in the experiment of Grion *et al.*. If we use the energy dependence of the free nucleon PIPP cross section [19] to rescale Rahav *et al.*'s result for ^{12}C to 240 MeV, we obtain $206 \pm 26\mu\text{b}$, in fair agreement with the value obtained using N_{eff} given in Table II.

We note that PIPP can only affect the low energy portion of the outgoing pion energy spectra. The estimated contributions will be shown when the results are presented in the next section.

IV. RESULTS

A. Doubly differential cross sections

A sample of the results of the present investigation will be displayed in this section² and some qualitative and semi-quantitative aspects of the measured cross sections will be discussed. The data will be compared with the predictions of two theoretical models in the next section.

Doubly differential cross sections for the $^6\text{Li}(\pi^+, \pi^-)$ process are shown in Figs. 3, 4, and 5 for incident energies 120, 180, and 240 MeV, respectively, and angles of observation between 25° and 130° . The $^6\text{Li}(\pi^-, \pi^+)$ cross sections (see Ref. [8]) are essentially identical in shape and magnitude and are not shown. The solid curves represent the distribution of events in four-body (outgoing pion, two nucleons, and residual nucleus) phase space and are normalized in each case to the area under the experimental spectrum. The phase space curves are seen to provide a good representation of the data at incident pion energy 120

² The complete set of data may be found in Ref. [8].

MeV and a poorer representation at the higher incident energies. The dashed curves in Fig. 5 indicate the estimated contribution of PIPP, assuming a phase-space distribution (as was found by Rahav *et al.* [22]). The angular dependence of the PIPP cross section was obtained from the measurements of Yuly *et al.* [4] and the normalization determined by the total cross section given in Table III.

Figure 6 shows the doubly differential cross sections for ${}^7\text{Li}(\pi^+, \pi^-)$ (solid symbols) and ${}^7\text{Li}(\pi^-, \pi^+)$ (open symbols) at 240 MeV incident energy. The dotted and dot-dashed curves indicate the estimated contributions of PIPP to the (π^+, π^-) and (π^-, π^+) cross sections, respectively. Comparing Figs. 5 and 6, it is seen that the shapes of the energy spectra are very similar at 240 MeV for the two Li isotopes. This similarity persists at the lower incident energies [8]. Although the ${}^7\text{Li}(\pi^+, \pi^-)$ and (π^-, π^+) cross sections are essentially identical in shape, the former is seen to be approximately a factor of three larger than the latter. This difference in magnitude will be discussed later in this section. It is also seen that the PIPP contribution is nearly identical for both reactions, and thus is relatively larger for ${}^7\text{Li}(\pi^-, \pi^+)$.

Figure 7 shows the doubly differential cross sections for ${}^9\text{Be}(\pi^+, \pi^-)$ (solid symbols) and ${}^9\text{Be}(\pi^-, \pi^+)$ (open symbols) at 180 MeV incident energy. The (π^+, π^-) cross section is seen to be approximately a factor of three larger than that for (π^-, π^+) .

As was stated earlier, one motivation for the study of inclusive DCX in light p -shell nuclei was to trace the A -dependence of the cross section – in particular the forward-angle cross section – from the double-peaked structure seen in ${}^3,4\text{He}$ to the single peak seen in ${}^{16}\text{O}$ and heavier nuclei. Figure 8 shows the doubly differential cross sections at 25° for 240 MeV (Fig. 8(a)) and 180 MeV (Fig. 8(b)) positive pions incident on ${}^4\text{He}$, ${}^6\text{Li}$, ${}^7\text{Li}$, ${}^9\text{Be}$, ${}^{12}\text{C}$, and ${}^{16}\text{O}$. Indeed, one observes a smooth progression in the shape of the spectra as A increases.³ At 240 MeV, the double-peaked structure is prominent in ${}^4\text{He}$, apparent in the Li isotopes, disappearing for ${}^9\text{Be}$, and is absent in ${}^{12}\text{C}$ and ${}^{16}\text{O}$. At 180 MeV the double-peaked structure is only seen in the ${}^4\text{He}$ spectrum, although the data for ${}^{6,7}\text{Li}$ and ${}^9\text{B}$ exhibit strength at high energy that does not appear in the ${}^{12}\text{C}$ and ${}^{16}\text{O}$ spectra. We note that in ${}^4\text{He}$ the double peaks are still visible at 150 MeV [6, 7], and in ${}^3\text{He}$ at all energies down to 120 MeV [4].

It is seen that the relative size of the PIPP contribution, shown as the dotted curves in

³ A very similar A -dependence is observed in the (π^-, π^+) cross sections.

Fig. 8(a), decreases with increasing A .

The origin of the double-peaked structure has been discussed previously (see, *e.g.*, Refs. [4, 7]), and has been argued to be consistent with a sequential single charge exchange mechanism. In the Δ resonance region the π -nucleon cross section is strongly forward- and backward-peaked. Two forward scatterings or two backward scatterings, which are favored over scattering at intermediate angles, can yield an outgoing DCX pion at forward angles: in the former case the pion emerges with high energy; in the latter case it emerges with lower energy. A theoretical model based on these ideas was developed by Kinney and successfully applied to DCX data on ${}^4\text{He}$ [6, 7] and, subsequently, ${}^3\text{He}$ [4]. Given the prominent double-peaked structure in the ${}^6\text{Li}$ cross section, we have extended the model to this nucleus, and will show the results in the next section.

Alqadi and Gibbs [24] have presented calculations for DCX in ${}^4\text{He}$ which they compare with the data given in Ref. [6]. These authors found that including PIPP in their intranuclear cascade model was essential to produce reasonable agreement with the data at 240 MeV, and suggest that this mechanism is largely responsible for the low-energy peak in the pion energy spectra. The contribution of PIPP for $A \geq 4$, obtained as discussed previously, is shown by the dashed curves in Fig. 8(a).

B. Angular distributions

As described in the previous section, the doubly differential cross sections were integrated to yield angular distributions (see Ref. [8]). A typical set of results, those for ${}^6\text{Li}$, is shown in Fig. 9. For this nucleus and the other nuclei investigated, the angular distribution is seen to be forward peaked at 240 MeV and to become more isotropic as the incident energy decreases. No significant difference is seen in the angular dependences of the (π^+, π^-) and (π^-, π^+) cross sections in those nuclei for which both were measured. Although the angular distributions are relatively featureless, their shape does exhibit a consistent A -dependence, becoming less forward-peaked as A increases. As a measure of the forward-peaking, the ratios of the cross sections measured at 25° and 130° for the (π^\pm, π^\mp) reactions at 240 MeV for $3 \leq A \leq 208$ were calculated and are displayed in Table III. The observed trend is consistent with the increased probability of absorption of forward-going pions as A increases; the DCX pion has a greater chance of escaping from the “rear” of a heavy nucleus. The unusually

small ratio seen for $^{208}\text{Pb}(\pi^-, \pi^+)$ may be attributable to the large excess of neutrons, with which the incoming π^- preferentially interacts, in this nucleus.

C. Total reaction cross sections

Total DCX reaction cross sections were determined as described in the previous section; the results for the light p -shell nuclei are given in Table IV. The quoted errors include statistics, systematics, and the uncertainties arising from the integration procedures. The numbers in parentheses for 240 MeV incident pions are the cross sections after the subtraction of the estimated contributions of PIPP.

For a self-conjugate nucleus, the (π^+, π^-) and (π^-, π^+) cross sections should be equal, apart from differences attributable to the different binding energies of the final state nuclei, which would affect primarily the high-energy end of the outgoing pion energy spectrum. The total cross sections for DCX in ^{16}O and ^{40}Ca were found to be equal within the experimental uncertainties [3], although the (π^-, π^+) cross section slightly exceeded the (π^+, π^-) cross section for ^{40}Ca . Table IV shows the two cross sections for ^6Li to be essentially equal within errors.

D. A -dependence of cross sections

Starting from the notion that double charge exchange proceeds by sequential single charge exchange scatterings competing with more probable reactions that either interrupt the sequence or scatter pions out of the nucleus before it starts, a “scaling rule” was found which organizes the A -dependence of the total cross section for both the (π^+, π^-) and (π^-, π^+) reactions [1]. According to this rule the total cross section for DCX should vary as

$$\sigma \sim A^{2/3}Q(Q-1)/(A-Q)(A-1), \quad (2)$$

where Q is the number of nucleons (N or Z) on which DCX occurs for a given incident pion charge (positive or negative); the factor $A^{2/3}$ is proportional to the projected area of the nucleus. Total DCX reaction cross sections in nuclei ranging in mass from ^6Li to ^{208}Pb are found substantially to obey this rule; only the isotopes of He violate it [1]. Given that the scaling rule is based on the classical transport of pions through nuclear matter, it is perhaps

surprising that the agreement is so good, especially for the light nuclei. The validity of the rule has recently been discussed by Buss *et al.* [25].

Let us examine the predictions of the scaling rule in more detail for the light p -shell nuclei. By comparing the (π^\pm, π^\mp) cross sections in ${}^6\text{Li}$ and ${}^7\text{Li}$, one can examine the effect of adding one neutron. For (π^+, π^-) one is adding a target nucleon; for (π^-, π^+) one is adding a source of competing reactions and the number of target nucleons is unchanged. Eq. (2) predicts the ratios $R(\pi^+, \pi^-) \equiv \sigma(\pi^+, \pi^-)_{7\text{Li}}/\sigma(\pi^+, \pi^-)_{6\text{Li}} = 1.85$ and $R(\pi^-, \pi^+) \equiv \sigma(\pi^-, \pi^+)_{7\text{Li}}/\sigma(\pi^-, \pi^+)_{6\text{Li}} = 0.69$. Note that in the absence of competing reactions $R(\pi^-, \pi^+)$ would be equal to unity. The observed ratios are given in Table V. The agreement between experiment and prediction for $R(\pi^-, \pi^+)$ is excellent at both 180 and 240 MeV; the observed values of $R(\pi^+, \pi^-)$ slightly exceed those predicted.

We can further examine the rule by comparing the (π^+, π^-) and (π^-, π^+) reactions in the $N \neq Z$ nuclei. In ${}^7\text{Li}$ and ${}^9\text{Be}$, the extra neutron should enhance the (π^+, π^-) reaction by providing more targets for the charge-exchange reactions and suppress the (π^-, π^+) reaction by providing more targets for the competing reactions. Eq. (2) predicts ratios of (π^+, π^-) to (π^-, π^+) of 2.67 in ${}^7\text{Li}$ and 2.08 in ${}^9\text{Be}$. The experimental ratios of the total cross sections, given in Table VI, are seen to agree well with these predictions at 240 MeV but to exceed them at 180 MeV.

To avoid additional uncertainties and assumptions, the ratios in Tables V and VI were obtained from the measured cross sections without the subtraction of PIPP. It was found that performing this subtraction does not alter the ratios outside their uncertainties and thus does not alter the conclusions drawn.

V. COMPARISON OF DATA WITH THEORETICAL MODELS

A. Intranuclear Cascade Calculation

In the intranuclear cascade calculation of Oset and collaborators [26, 27, 28, 29], the probabilities for pion quasi-elastic scattering and absorption are computed using a microscopic model in which the pion is propagated classically through the nucleus. Quasi-elastic single charge exchange as well as non-charge exchange interactions are allowed, and thus this model can be employed to generate DCX cross sections based on the sequential single

charge exchange mechanism. The calculation is performed in infinite nuclear matter, invoking the local density approximation to evaluate the reaction probabilities. Further details of the calculation may be found in Ref. [8]. Results of this calculation have previously been compared with DCX data on ^{16}O , ^{40}Ca , ^{103}Rh , and ^{208}Pb [3, 28, 29]. Ref. [29] also contains some comparisons with results of the present experiment for ^9Be and ^{12}C .

The predictions of this model are compared with the present data for $^6\text{Li}(\pi^+, \pi^-)$ and $^7\text{Li}(\pi^+, \pi^-)$ at 240 MeV in Figs. 10 and 11, respectively. A persistent feature of the calculations is a low-energy peak that is not seen in the data. A hint of the double-peaked structure seen in the forward-angle spectra does appear in the calculation, but the high energy peak is at too high an energy and of insufficient amplitude to match that observed. Comparison of this calculation with data on ^9Be shows qualitatively similar results – see Fig. 6 of Ref. [29]. If one attributes the measured strength in the low-energy region of the forward angle spectra to PIPP, as suggested by the work of Alqadi and Gibbs [24], then the disagreement between the measured and calculated doubly-differential cross sections is even more striking.

Given the disparities in the measured and calculated doubly differential cross sections, comparison of the integrated cross sections may not be very meaningful. However, it can be seen by inspection of the energy spectra that the magnitude of the cross section is better reproduced by the theory for ^7Li than for ^6Li . Fig. 12 shows the theory and measurement for $^7\text{Li}(\pi^-, \pi^+)$ at 240 MeV. The comparison of theory and experiment is qualitatively similar to that for $^7\text{Li}(\pi^+, \pi^-)$. Calculations have also been performed [8] at 180 MeV and 120 MeV. Although the calculation reproduces the approximate isotropy of the cross sections at these lower energies, quantitative comparisons are on the whole no more successful than at the higher energy. But perhaps it is not surprising that a calculation designed for heavy nuclei cannot predict the details of the DCX process in these very light nuclei. Vicente-Vacas and Oset [29] comment that a major weakness of their calculation is the fact that the model [27] predicts narrower quasi-elastic scattering peaks than are observed, and that this might have a bearing on the discrepancy seen between theory and measurement for light nuclei.

B. Non-static Sequential Single Charge Exchange Model

We next compare our data with the predictions of a model developed by Kinney [6] based on the sequential single charge exchange mechanism. This treatment is an extension of some

of the work of van Loon [30] and relies on the formalism developed by Thies [31] to describe inelastic, multistep reactions with quantum-mechanical transport theory.

The essential features of the calculation are discussed in Ref. [7]; an extended description is contained in Ref. [6]. In this model the incident pion interacts sequentially with two like-charge nucleons only, and thus only the leading, or “double scattering”, term in the transition matrix is used, *i.e.*,

$$T = \sum_{i=1}^A \sum_{j \neq i}^A t_i G_0 t_j, \quad (3)$$

where the t_i are the in-medium transition operators (t -matrices) for scattering from the i th nucleon, and G_0 is the in-medium pion propagator. What distinguishes this calculation from simpler folding models [17, 30] is the non-static treatment of the πN interaction, which is important because in the energy region of the Δ resonance, the interaction between the pion and the nucleon varies strongly with pion-nucleon relative energy. Also, the binding of the nucleons is taken into account via an approximate prescription.

The predictions of this model have been compared with DCX data on ${}^3\text{He}$ [4] and ${}^4\text{He}$ [7]. Here we extend the calculations to ${}^6\text{Li}$, and accordingly must modify the initial state wave function to take into account the presence of the p -shell proton and neutron. We describe the ${}^6\text{Li}$ nucleus by a product of $(1s)$ and $(1p)$ harmonic oscillator wave functions: $(1s)^2(1p)$. The DCX amplitude is summed over the three possible sequences of first and second interactions: (ss) , (sp) , and (ps) . The (ss) sequence is seen to contribute about 25% and the combined (sp) and (ps) sequences about 75% to the total amplitude [8].

In Fig. 13 we compare the results of this calculation with the measured doubly differential cross section at five angles for incident pion energy 240 MeV, with two assumptions for the value of the average nuclear potentials U_1 and U_2 at the first and second scattering, respectively. The solid curves (lower branches) represent the calculation for $U_1 = U_2 = -30$ MeV; the dashed curves (lower branches) that for $U_1 = U_2 = 0$. The sequential scattering model does indeed predict a high energy peak in the forward angle cross sections that is reasonably close, both in magnitude and in position in energy, to that seen in the data; the evolution of this peak to larger angles is also quite well reproduced.

Whereas for ${}^3\text{He}$ and ${}^4\text{He}$ this calculation predicted a double-peaked spectrum at forward angles that agreed fairly well with the data, the inclusion of a p -shell nucleon seems to greatly diminish the low-energy peak, compared with the data. The question arises as to

whether the primary origin of the observed low-energy peaks at 240 MeV in the light p -shell DCX data is in fact PIPP, as was suggested by Alqadi and Gibbs [24] for DCX in ${}^4\text{He}$. The upper branches of the solid and dashed curves were obtained by adding the estimated PIPP cross sections from Fig. 5 (which assume a phase-space distribution) to the calculated DCX cross sections. The agreement with the data is seen to be surprisingly good, and may be fortuitous, given the simplicity of the assumptions made for both DCX and PIPP.

The DCX calculations in Fig. 13 show very little dependence on the nuclear potential. However, when the calculation is compared to the data at 25° for incident energies 120, 180, and 240 MeV (Fig. 14), we see that the choice of the potential has a significant effect. Whereas the calculation for $U_1 = U_2 = 0$ provides a fairly good representation of the magnitude of the cross section at all three energies, that for $U_1 = U_2 = -30$ MeV produces a prediction that is approximately three times too large at 180 MeV and five times too large at 120 MeV. The same phenomenon was seen in the comparison of this model with data on ${}^3\text{He}$ and ${}^4\text{He}$: only by setting both potentials to zero could the magnitude of the predicted cross section be brought close to the data at 120 and 180 MeV.

VI. SUMMARY AND CONCLUSIONS

A systematic study of the inclusive DCX process in light p -shell nuclei has been performed for incident pion energies between 120 MeV and 240 MeV. The relative magnitudes of the cross sections were found to be roughly consistent with a “scaling rule” [1] derived by assuming DCX to proceed via two sequential single charge exchange (SSCX) reactions in competition with other processes.

The data are compared with the predictions of two theoretical models: an intranuclear cascade model of Oset and collaborators [26, 27, 28, 29] and a model developed by Kinney [6] based on the SSCX mechanism. Although one would expect the model of Oset, which allows multiple interactions, to provide a better reproduction of the data, this does not appear to be the case. In particular, the strength at low outgoing pion energies, which one would expect to arise from multiple interactions, is calculated to be much larger than that seen in the data. Either the effect of these interactions has been overestimated, or one or more of the approximations in this calculation has produced a distortion of the spectrum.

The calculation of Kinney [6] provides an overall better representation of the data for ${}^6\text{Li}$,

particularly if PIPP is included. Although a double-peaked structure in the forward angle spectra is expected if SSCX is the dominant mechanism, the structure seen for ${}^6\text{Li}$ and ${}^7\text{Li}$ at 240 MeV probably contains a contribution from PIPP. We note that the data at 180 MeV for these nuclei do not exhibit a low-energy peak.

However, PIPP cannot provide the complete explanation, since for ${}^3\text{He}$ and ${}^4\text{He}$ the low-energy peak persists to energies well below the PIPP threshold. We suggest that both SSCX and PIPP mechanisms are at work to produce pions of charge opposite to that of the incident beam. The double peak signature of SSCX appears clearly in ${}^3\text{He}$ and ${}^4\text{He}$ owing to the simplicity of these nuclei. As A increases, the presence of additional nucleons affords the possibility of more than two interactions, and “washes out” this structure.

In conclusion, the work reported in this paper completes a systematic study of the A -dependence of the inclusive double charge exchange process at intermediate energies. Results for lighter [4, 7] and heavier [3] nuclei have been published previously. Although many qualitative features of the inclusive DCX process are now fairly well understood, a quantitative theoretical description of the measured cross sections has yet to be achieved.

VII. ACKNOWLEDGMENTS

This work was supported in part by funds provided by the U.S. Department of Energy. We acknowledge the contributions of D. Cors, S. Høibråten, P. Mansky, and C. Schermer to the data-taking phase of this experiment. We wish to thank E. Oset for making his code available to us and for guidance in its use. We are grateful to M. Yuly for insightful discussions of the data analysis procedures and for a careful reading of the final manuscript. T. Akdogan provided valuable assistance in the preparation of the figures.

-
- [1] P. A. M. Gram, S. A. Wood, E. R. Kinney, S. Høibråten, P. Mansky, J. L. Matthews, T. Soos, G. A. Rebka, Jr., and D. A. Roberts, *Phys. Rev. Lett.* **62**, 1837 (1989).
 - [2] R. E. Mischke, A. Blomberg, P. A. M. Gram, J. Jansen, J. Zichy, J. Bolger, E. Boschitz, C. H. Q. Ingram, and G. Pröbstle, *Phys. Rev. Lett.* **44**, 1197 (1980).
 - [3] S. A. Wood, J. L. Matthews, E. R. Kinney, P. A. M. Gram, G. A. Rebka, Jr., and D. A. Roberts, *Phys. Rev. C* **46**, 1903 (1992).

- [4] M. Yuly, W. Fong, E. R. Kinney, C. J. Maher, J. L. Matthews, T. Soos, J. Vail, M. Y. Wang, S. A. Wood, P. A. M. Gram, G. A. Rebka, Jr. and D. A. Roberts, *Phys. Rev. C* **55**, 1848 (1997).
- [5] E. R. Kinney, J. L. Matthews, P. A. M. Gram, D. W. MacArthur, E. Piasezky, G. A. Rebka, Jr., and D. A. Roberts, *Phys. Rev. Lett.* **57**, 3152 (1986).
- [6] E. R. Kinney, Los Alamos National Laboratory Report No. LA-11417-T, 1988.
- [7] E. R. Kinney, J. L. Matthews, P. A. M. Gram, D. W. MacArthur, E. Piasezky, G. A. Rebka, Jr., and D. A. Roberts, *Phys. Rev. C* **72**, 044608 (2005).
- [8] W. Fong, Ph.D. Thesis, Massachusetts Institute of Technology, 1994.
- [9] W. Fong, J. L. Matthews, M. L. Dowell, E. R. Kinney, S. A. Wood, P. A. M. Gram, G. A. Rebka, Jr., and D. A. Roberts, *Few-Body Systems Suppl.* **9**, 187 (1995).
- [10] L. Gilly, M. Jean, R. Meunier, M. Spighel, J. P. Stroot, P. Duteil, and A. Rode, *Phys. Lett.* **11**, 244 (1964).
- [11] L. Gilly, M. Jean, R. Meunier, M. Spighel, J. P. Stroot, and P. Duteil, *Phys. Lett.* **19**, 335 (1965).
- [12] Yu. A. Batusov, S. A. Bunyatov, V. M. Sidorov, and V. A. Yarba, *Sov. J. Nucl. Phys.* **3**, 223 (1966).
- [13] J. P. Massué, Y. Sakamoto, Yu. A. Batusov, and P. Cüer, *Nucl. Phys.* **B29**, 515 (1971).
- [14] V. S. Evseev, V. S. Kurbatov, V. M. Sidorov, V. B. Belyaev, J. Wrzeczionko, M. Daum, R. Frosch, J. McCulloch, and E. Steiner, *Nucl. Phys.* **A352**, 379 (1981).
- [15] B. M. Abramov, L. Alvarez-Ruso, Yu. A. Borodin, S. A. Bulychjov, M. J. Vicente Vacas, I. A. Dukhovskoy, A. P. Krutenkova, V. V. Kulikov, M. A. Matsyuk, and E. N. Turdakina, *Yadernaya Fizika* **68**, 1336 (2005) [*Physics of Atomic Nuclei* **68**, 1283 (2005)].
- [16] J. B. Walter and G. A. Rebka, Jr., Los Alamos National Laboratory Technical Report No. LA-7731-MS (1979).
- [17] S. A. Wood, Los Alamos National Laboratory Report No. LA-9932-T, 1983.
- [18] D. Ashery, I. Navon, G. Azuelos, H. K. Walter, H. J. Pfeiffer, and F. W. Schlepütz, *Phys. Rev. C* **23**, 2173 (1981).
- [19] C. W. Bjork *et al.*, *Phys. Rev. Lett.* **44**, 62 (1980).
- [20] E. Piasezky, P. A. M. Gram, D. W. MacArthur, G. A. Rebka, Jr., C. A. Bordner, S. Hoibraten, E. R. Kinney, J. L. Matthews, S. A. Wood, and J. Lichtenstadt, *Phys. Rev.*

- Lett. **53**, 540 (1984); J. Lichtenstadt, D. Ashery, S. A. Wood, E. Piasetzky, P. A. M. Gram, D. W. MacArthur, R. S. Bhalerao, L. C. Liu, G. A. Rebka, Jr. and D. Roberts, Phys. Rev. C **33**, 655 (1986).
- [21] F. Bonutti *et al.*, Nucl. Phys. **A677**, 213 (2000).
- [22] A. Rahav *et al.*, Phys. Rev. Lett **66**, 1279 (1991).
- [23] N. Grion *et al.*, Nucl. Phys. **A492**, 509 (1989).
- [24] M. Alqadi and W. R. Gibbs, Phys. Rev. C **65**, 044609 (2002).
- [25] O. Buss, L. Alvarez-Ruso, A. B. Larionov, and U. Mosel, Phys. Rev. C **74**, 044610 (2006).
- [26] E. Oset, L. L. Salcedo, and D. Strottman, Phys. Lett. B **165**, 13 (1985).
- [27] L. L. Salcedo, E. Oset, M. J. Vicente-Vacas, and C. García-Recio Nucl. Phys. **A484**, 557 (1988).
- [28] M. J. Vicente, E. Oset, L. L. Salcedo, and C. García-Recio, Phys. Rev. C **39**, 209 (1989).
- [29] M. Vicente-Vacas and E. Oset, in *Second LAMPF International Workshop on Pion-Nucleus Double Charge Exchange*, Los Alamos, 1989, edited by W. R. Gibbs and M. J. Leitch (World Scientific, Singapore, 1990), p. 120.
- [30] J. van Loon, Master's Thesis, Free University, Amsterdam, 1985.
- [31] M. Thies, Ann. Phys. (N.Y.) **123**, 411 (1979).

TABLE I: Systematic uncertainties in the experiment.

Systematic uncertainties (%)			
Incident Beam	Normalization	Angle-dependent ^a	Overall ^b
120 MeV π^+	4.8	1.3	5.0
120 MeV π^-	5.1	5.3	7.4
180 MeV π^+	6.5	5.1	8.3
180 MeV π^-	6.4	1.0	6.4
240 MeV π^+	6.2	1.9	6.5
240 MeV π^-	6.8	1.6	7.0

^aAngle-dependent uncertainty due to variation in ionization chamber response (see text).

^bIncludes angle-dependent and normalization uncertainties only. The uncertainties which depend on the energy of observation are included along with the statistical uncertainties in the plotted error bars.

TABLE II: Estimated cross sections (μb) for pion-induced pion production by 240 MeV incident pions. The result for ^4He is taken from Ref. [7]. The quoted uncertainties reflect only the uncertainty in the $\pi^-p \rightarrow \pi^+\pi^-n$ cross section, except in the case of $^7\text{Li}(\pi^+, \pi^-)$ where there is an additional uncertainty arising from the determination of N_{eff} .

Target nucleus	(π^+, π^-)	(π^-, π^+)
^4He	128 ± 8	
^6Li	190 ± 11	190 ± 11
^7Li	252 ± 27	190 ± 11
^9Be	245 ± 15	219 ± 13
^{12}C	268 ± 16	
^{16}O	309 ± 19	

TABLE III: Ratio of the differential cross section at 25° to that at 130° , for 240 MeV incident pions.

Target nucleus	(π^+, π^-)	(π^-, π^+)
^3He		2.61 ± 0.19
^4He	2.92 ± 0.14	2.67 ± 0.30
^6Li	1.82 ± 0.07	1.84 ± 0.07
^7Li	1.74 ± 0.06	1.66 ± 0.06
^9Be	1.51 ± 0.02	1.57 ± 0.03
^{12}C	1.27 ± 0.02	
^{16}O	1.18 ± 0.04	1.33 ± 0.05
^{40}Ca	0.99 ± 0.03	1.01 ± 0.03
^{103}Rh	0.78 ± 0.02	0.77 ± 0.02
^{208}Pb	0.82 ± 0.02	0.54 ± 0.01

TABLE IV: Total DCX reaction cross sections for ^6Li , ^7Li , ^9Be , and ^{12}C .

Incident Beam	Reaction cross sections (mb)			
	^6Li	^7Li	^9Be	^{12}C
120 MeV π^+	0.31 ± 0.03	0.80 ± 0.05	0.94 ± 0.04	2.17 ± 0.17
120 MeV π^-		0.17 ± 0.02	0.34 ± 0.02	
180 MeV π^+	1.05 ± 0.08	2.43 ± 0.18	3.15 ± 0.22	
180 MeV π^-	0.88 ± 0.07	0.60 ± 0.04	0.95 ± 0.07	
240 MeV π^+	$1.87(1.68) \pm 0.11$	$4.00(3.75) \pm 0.24$	$4.28(4.03) \pm 0.23$	$3.73(3.46) \pm 0.25$
240 MeV π^-	$1.76(1.57) \pm 0.12$	$1.36(1.17) \pm 0.09$	$2.22(2.00) \pm 0.10$	

TABLE V: Ratios of ${}^7\text{Li}$ to ${}^6\text{Li}$ total DCX reaction cross sections.

Incident Energy (MeV)	$R(\pi^+, \pi^-)^a$		$R(\pi^-, \pi^+)^a$	
	Expt.	Scal. Rule	Expt.	Scal. Rule
180	2.31 ± 0.25	1.85	0.68 ± 0.07	0.69
240	2.14 ± 0.19	1.85	0.77 ± 0.08	0.69

^aThe ratios are $R(\pi^\pm, \pi^\mp) \equiv \sigma(\pi^\pm, \pi^\mp)_{{}^7\text{Li}} / \sigma(\pi^\pm, \pi^\mp)_{{}^6\text{Li}}$.

TABLE VI: Ratios of (π^+, π^-) to (π^-, π^+) total reaction cross sections for ${}^7\text{Li}$ and ${}^9\text{Be}$.

Incident Energy (MeV)	${}^7\text{Li}$		${}^9\text{Be}$	
	Expt.	Scal. Rule	Expt.	Scal. Rule
180	4.05 ± 0.40	2.67	3.32 ± 0.34	2.08
240	2.94 ± 0.26	2.67	1.93 ± 0.14	2.08

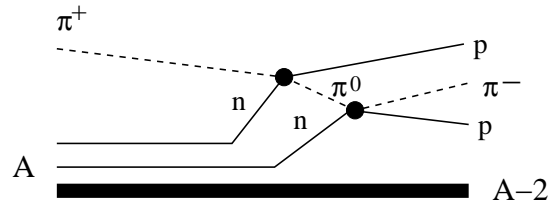


FIG. 1: Schematic diagram of the sequential single charge exchange mechanism for the (π^+, π^-) reaction.

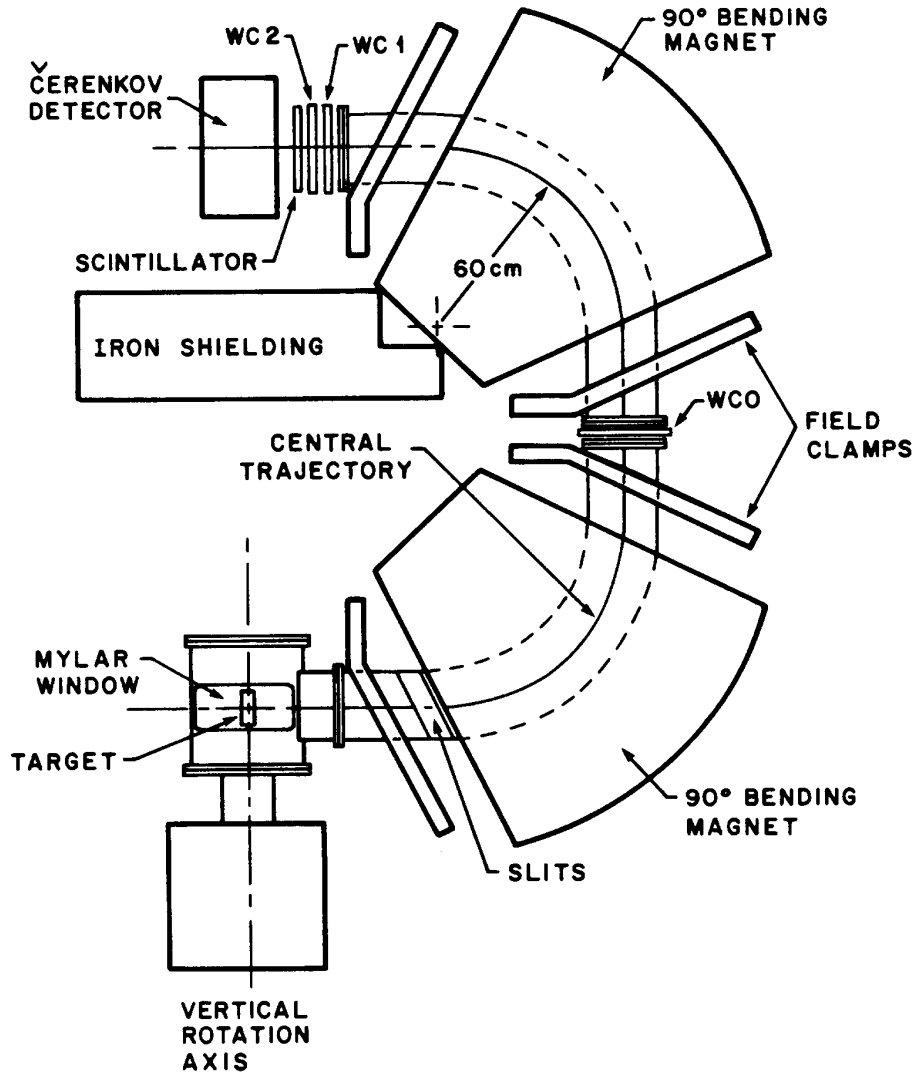


FIG. 2: Drawing of the 180° vertical bend, double focussing magnetic spectrometer. Pions travel through vacuum from the target, through two 90° dipole magnets, to the focal plane. There is a 2.5 cm break in the vacuum for WC0, the mid-spectrometer wire chamber, which is used to require that a particle traverses the entire spectrometer. Particle trajectories are traced back to the focal plane using information from two wire chambers, WC1 and WC2. The scintillator is used to distinguish positive pions from protons, as well as to provide TOF information. The Čerenkov detector separates pions from electrons and positrons.

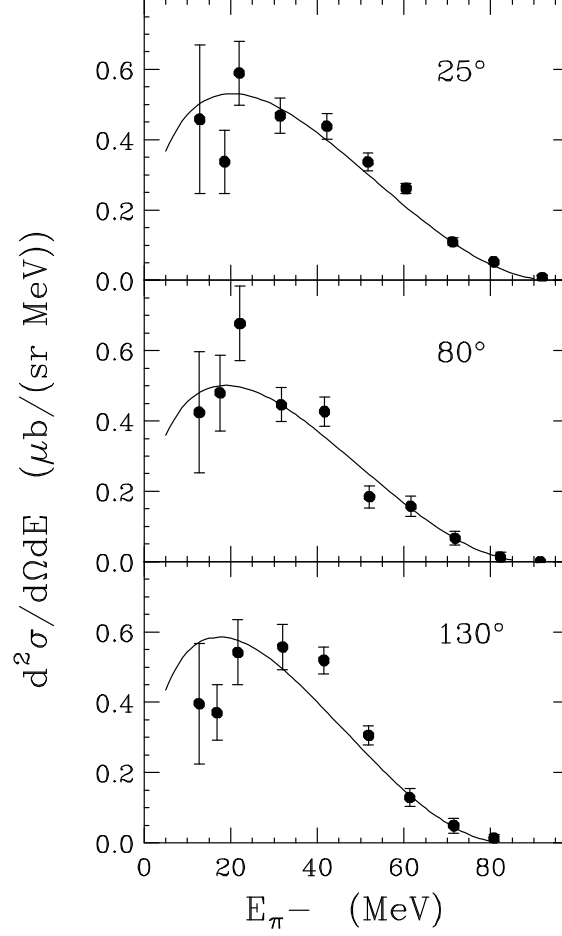


FIG. 3: Doubly differential cross sections for ${}^6\text{Li}(\pi^+, \pi^-)$ at incident energy 120 MeV for laboratory angles 25° , 80° , and 130° . The uncertainties indicated include the statistical uncertainty and the systematic uncertainties which depend on the outgoing pion energy. The solid curves represent the distribution of events in four-body phase space.

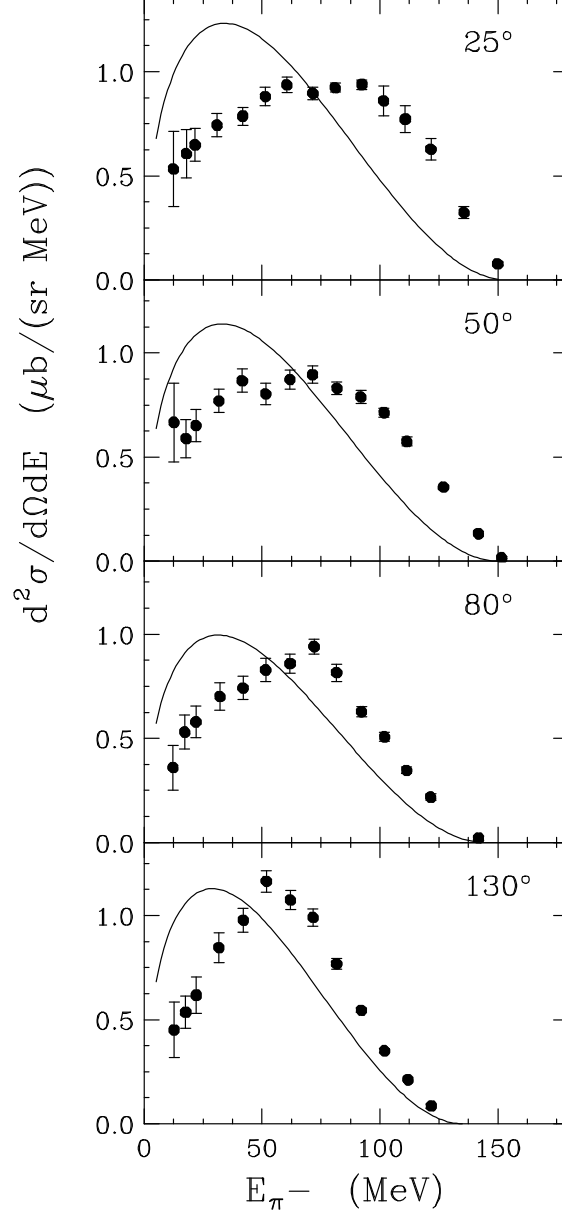


FIG. 4: Doubly differential cross sections for ${}^6\text{Li}(\pi^+, \pi^-)$ at incident energy 180 MeV for laboratory angles 25° , 50° , 80° , and 130° . The uncertainties indicated include the statistical uncertainty and the systematic uncertainties which depend on the outgoing pion energy. The solid curves represent the distribution of events in four-body phase space.

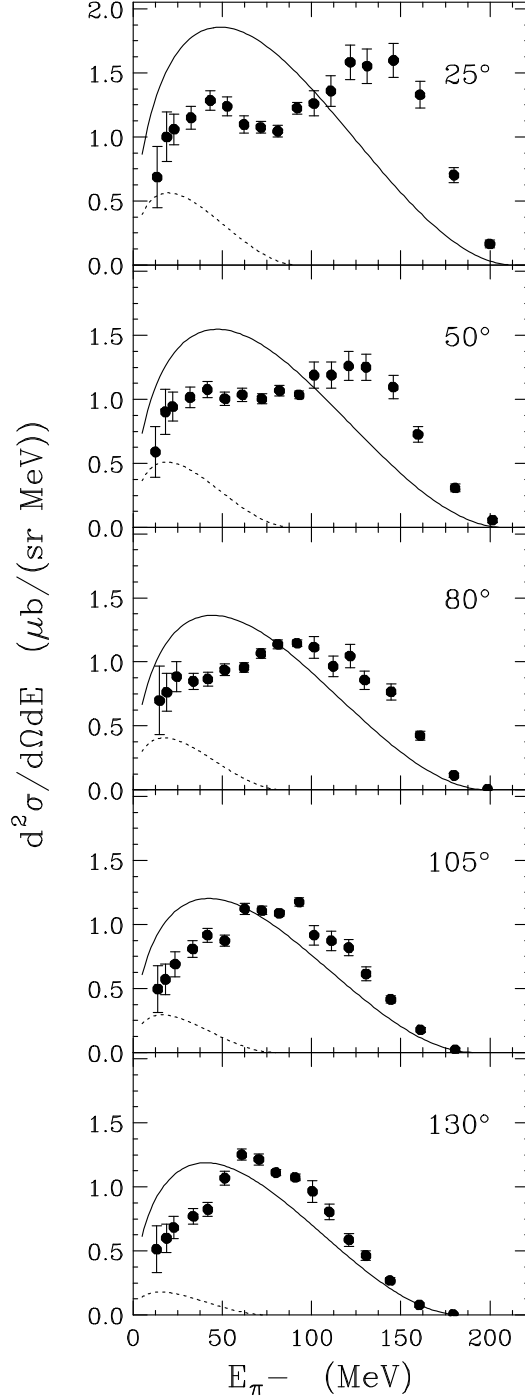


FIG. 5: Doubly differential cross sections for ${}^6\text{Li}(\pi^+, \pi^-)$ at incident energy 240 MeV for laboratory angles 25° , 50° , 80° , 105° , and 130° . The uncertainties indicated include the statistical uncertainty and the systematic uncertainties which depend on the outgoing pion energy. The solid curves represent the distribution of events in four-body phase space; the dashed curves indicate the estimated contributions of PIPP (see text).

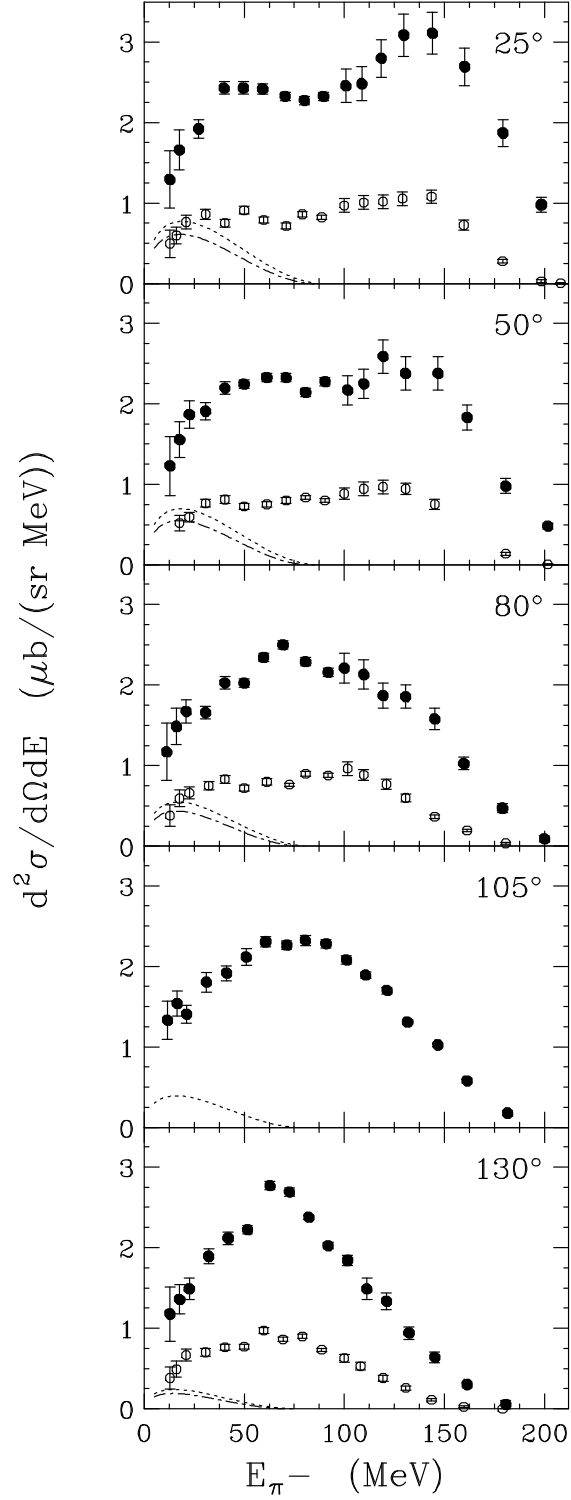


FIG. 6: Doubly differential cross sections for ${}^7\text{Li}(\pi^+, \pi^-)$ (solid symbols) and ${}^7\text{Li}(\pi^-, \pi^+)$ (open symbols) at 240 MeV incident energy. The dotted and dot-dashed curves indicate the estimated contributions of PIPP for (π^+, π^-) and (π^-, π^+) , respectively.

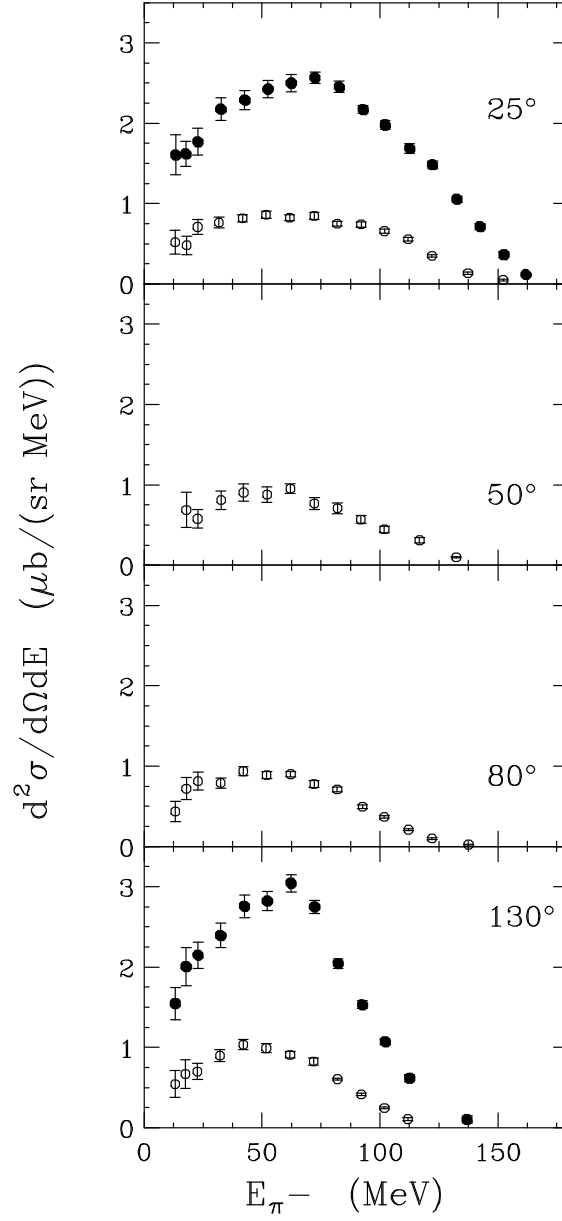


FIG. 7: Doubly differential cross sections for ${}^9\text{Be}(\pi^+, \pi^-)$ (solid symbols) and ${}^9\text{Be}(\pi^-, \pi^+)$ (open symbols) at 180 MeV incident energy.

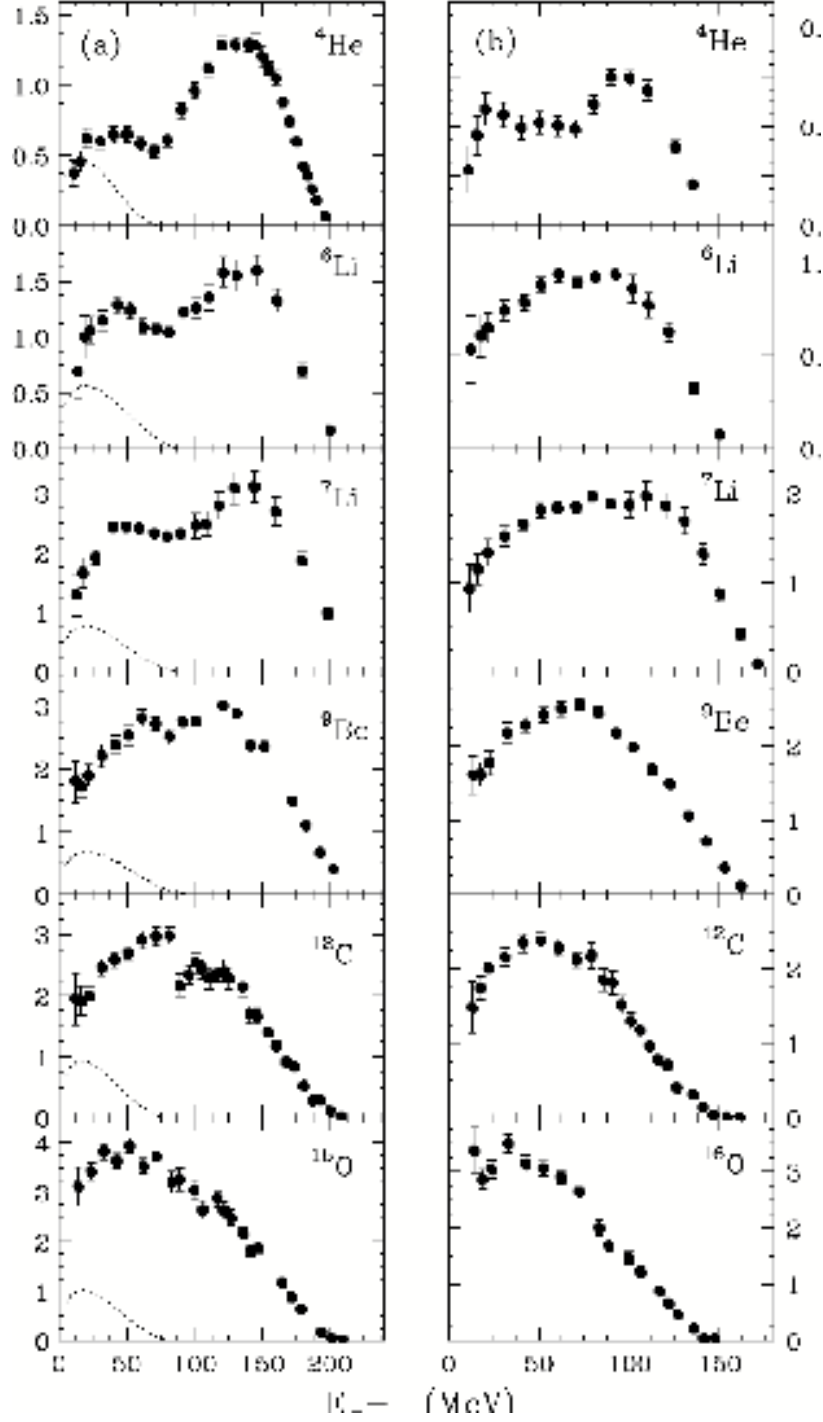


FIG. 8: Doubly differential cross sections at 25° for (a) 240 MeV and (b) 180 MeV positive pions incident on ^4He , ^6Li , ^7Li , ^9Be , ^{12}C , and ^{16}O . The dotted curves in (a) represent the estimated contribution of PIPP (see text).

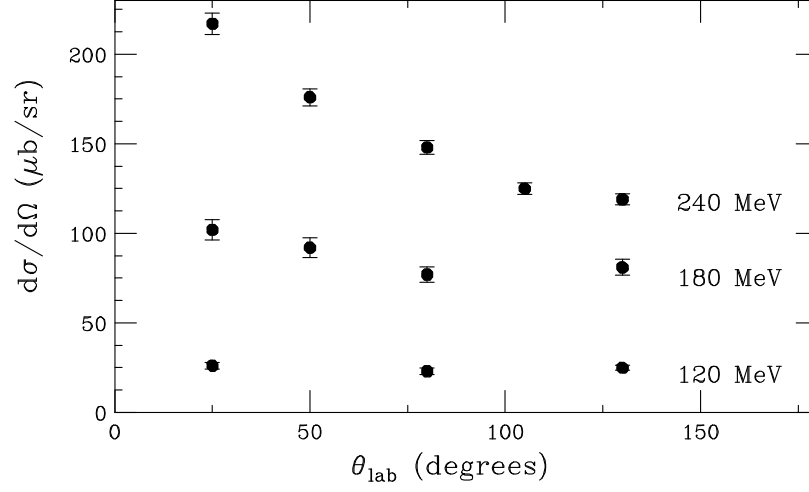


FIG. 9: Angular distributions for ${}^6\text{Li}(\pi^+, \pi^-)$ at 120, 180, and 240 MeV. The uncertainties shown include the statistical uncertainty, the uncertainties arising from the extrapolation and integration procedure (see text), and the systematic uncertainties which depend on the outgoing pion energy and angle.

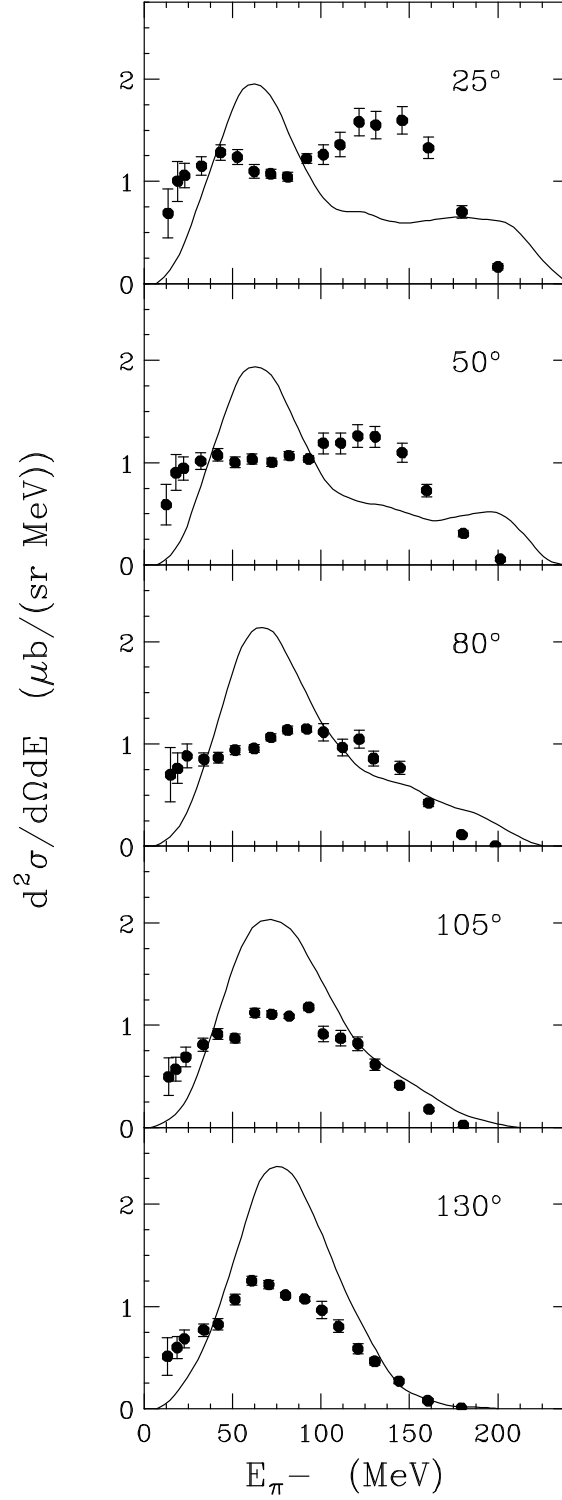


FIG. 10: Comparison of doubly differential cross section for ${}^6\text{Li}(\pi^+, \pi^-)$ at incident energy 240 MeV with prediction of the intranuclear cascade calculation of Oset (see text).

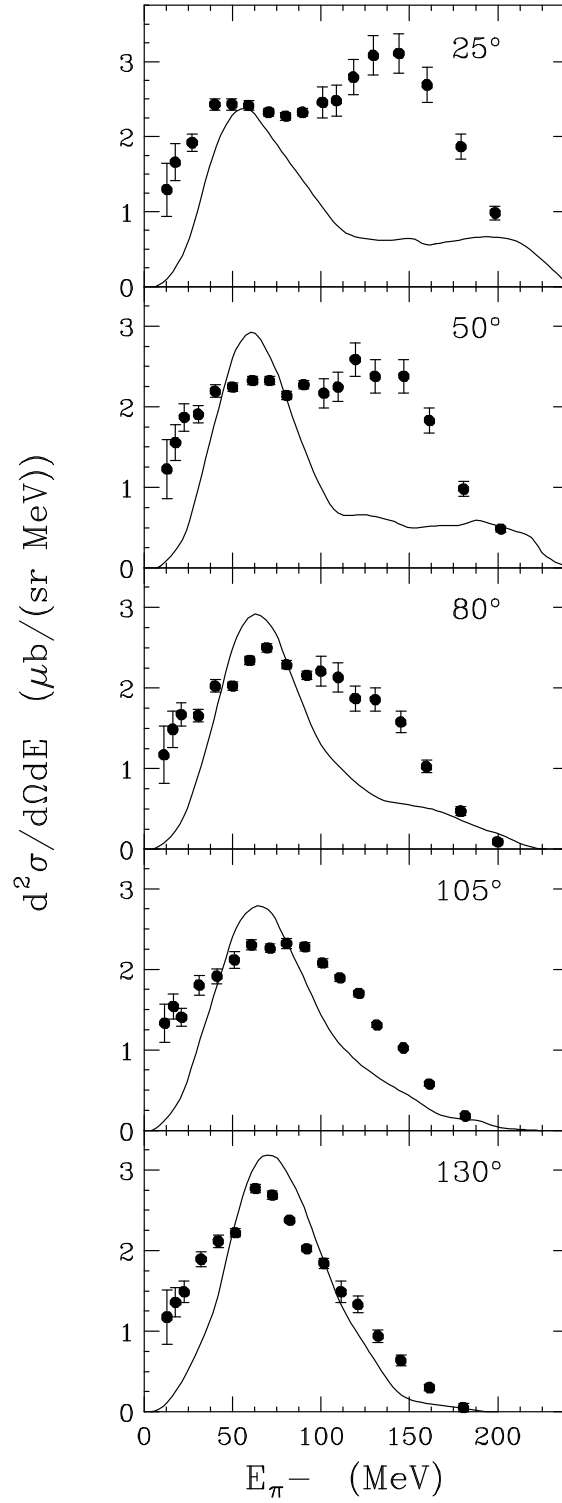


FIG. 11: As Fig. 10 for ${}^7\text{Li}(\pi^+, \pi^-)$.

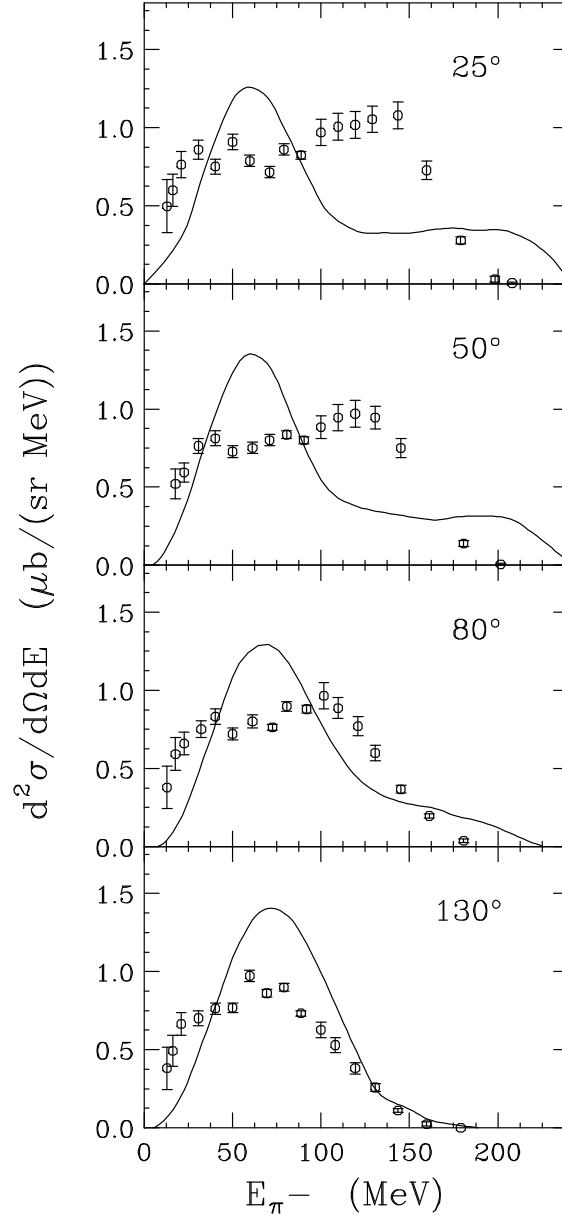


FIG. 12: As Fig. 10 for ${}^7\text{Li}(\pi^-, \pi^+)$.

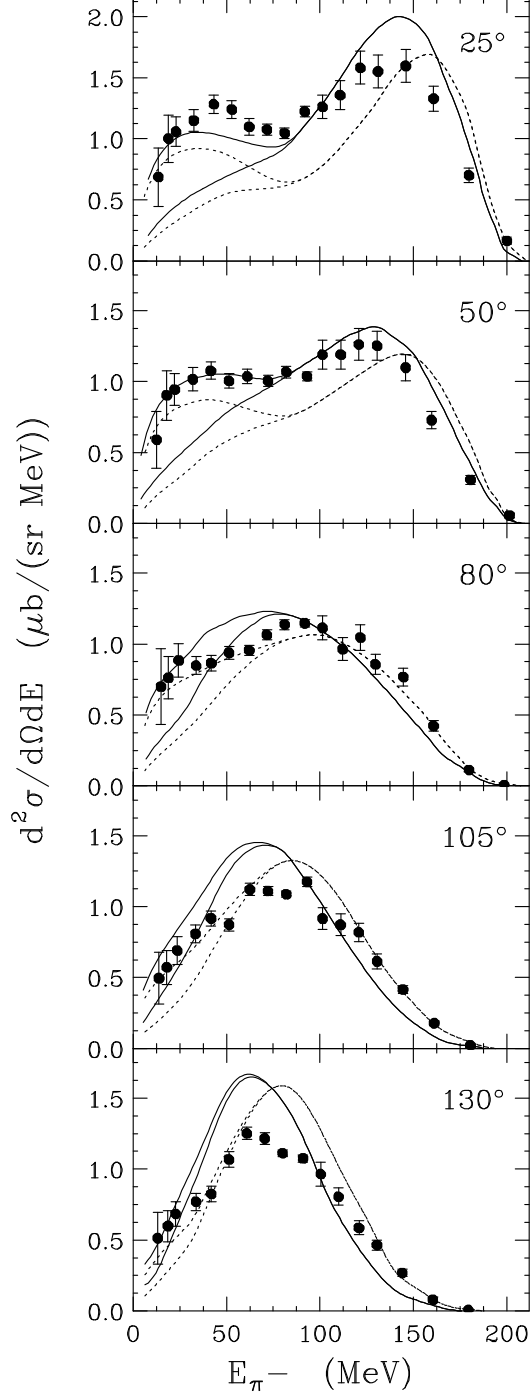


FIG. 13: Comparison of doubly differential cross sections for ${}^6\text{Li}(\pi^+, \pi^-)$ at incident energy 240 MeV and laboratory angles 25° , 50° , 80° , 105° , and 130° with predictions of a non-static sequential single charge exchange model (lower branches of curves). The average nuclear potentials are $U_1 = U_2 = -30$ MeV (solid curves), $U_1 = U_2 = 0$ MeV (dotted curves). The upper branches of the curves include PIPP (see text).

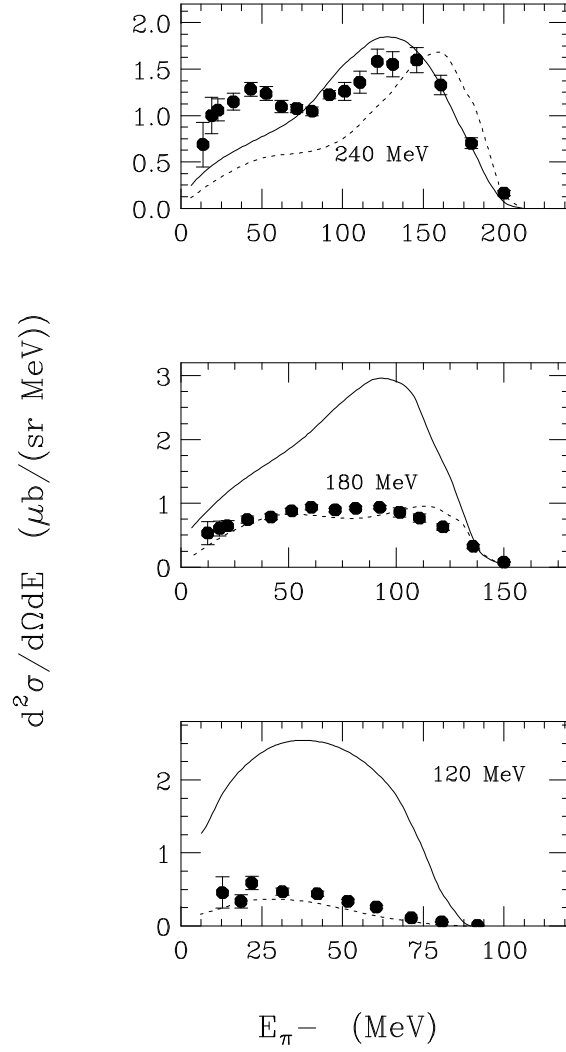


FIG. 14: Comparison of doubly differential cross section for ${}^6\text{Li}(\pi^+, \pi^-)$ at 25° for incident energies 120, 180, and 240 MeV with prediction of a non-static sequential single charge exchange model. The curves are as in Fig. 13.

This figure "fig08.gif" is available in "gif" format from:

<http://arxiv.org/ps/nucl-ex/0701002v1>